



HAL
open science

Beta bursts question the ruling power for brain-computer interfaces

Sotirios Papadopoulos, Maciej J Szul, Marco Congedo, James J Bonaiuto,
Jérémie Mattout

► **To cite this version:**

Sotirios Papadopoulos, Maciej J Szul, Marco Congedo, James J Bonaiuto, Jérémie Mattout. Beta bursts question the ruling power for brain-computer interfaces. 2023. hal-04213112

HAL Id: hal-04213112

<https://hal.science/hal-04213112>

Preprint submitted on 21 Sep 2023

HAL is a multi-disciplinary open access archive for the deposit and dissemination of scientific research documents, whether they are published or not. The documents may come from teaching and research institutions in France or abroad, or from public or private research centers.

L'archive ouverte pluridisciplinaire **HAL**, est destinée au dépôt et à la diffusion de documents scientifiques de niveau recherche, publiés ou non, émanant des établissements d'enseignement et de recherche français ou étrangers, des laboratoires publics ou privés.



Distributed under a Creative Commons Attribution - NoDerivatives 4.0 International License

1 Beta bursts question the ruling power for brain-computer 2 interfaces

3

4 Sotirios Papadopoulos^{1,2,3,*}, Maciej J Szul^{1,3}, Marco Congedo⁴, James J Bonaiuto^{1,3,†}, Jérémie
5 Mattout^{1,2,†}

6 ¹ University Lyon 1, Lyon, France

7 ² Lyon Neuroscience Research Center, CRNL, INSERM U1028, CNRS, UMR5292, Lyon,
8 France

9 ³ Institut de Sciences Cognitives Marc Jeannerod, CNRS, UMR5229, Lyon, France

10 ⁴ GIPSA-lab, University Grenoble Alpes, CNRS, Grenoble-INP, Grenoble, France

11

12 ***correspondence:** Sotirios Papadopoulos

13 **Email:** sotirios.papadopoulos@univ-lyon1.fr

14 †these two authors contributed equally

15 **Keywords:** beta bursts, brain-computer interface (BCI), decoding, electroencephalography
16 (EEG), motor imagery (MI)

17

18 **Abstract**

19 Current efforts to build reliable brain-computer interfaces (BCI) span multiple axes from
20 hardware, to software, to more sophisticated experimental protocols, and personalized
21 approaches. However, despite these abundant efforts, there is still room for significant
22 improvement. We argue that a rather overlooked direction lies in linking BCI protocols with
23 recent advances in fundamental neuroscience. In light of these advances, and particularly the
24 characterization of the burst-like nature of beta frequency band activity and the diversity of beta
25 bursts, we revisit the role of beta activity in “left vs. right hand” motor imagery tasks. Current
26 decoding approaches for such tasks take advantage of the fact that motor imagery generates
27 time-locked changes in induced power in the sensorimotor cortex, and rely on band-pass
28 filtered power changes or covariance matrices which also describe co-varying power changes in
29 signals recorded from different channels. Although little is known about the dynamics of beta
30 burst activity during motor imagery, we hypothesized that beta bursts should be modulated in a
31 way analogous to their activity during performance of real upper limb movements. We show that
32 classification features based on patterns of beta burst modulations yield decoding results that
33 are equivalent to or better than typically used beta power across multiple open
34 electroencephalography datasets, thus providing insights into the specificity of these bio-
35 markers.

36

37

38 **Introduction**

39 Neural interfaces, and in particular brain-computer interfaces (BCI), have long been
40 conceptualized as effective means of surmounting disabilities for patients suffering from various
41 diseases and traumas, while transhumanist philosophy sees BCI [1] as a way to enhance the
42 capabilities of our bodies and brains. To achieve such goals, a multidisciplinary approach is
43 crucial. Over the past few decades, an increasing number of research groups from diverse
44 fields have been striving towards several objectives, from laying the foundations of BCI [2–6] to
45 improving their reliability [7,8] and applicability under more naturalistic settings [8–10].

46 Although we are still far from achieving goals like those portrayed in science fiction, a few real-
47 world BCI applications are currently deployed. Most applications revolve around selected
48 groups of patients [12–20], improving their ability to interact with their environment. Such
49 applications usually form part of studies that employ invasive recording techniques in an attempt
50 to acquire high-quality brain signals [21,22]. Invasive techniques provide higher signal-to-noise
51 ratio, spatial specificity and frequency resolution compared to non-invasive techniques, trading
52 off the availability of the subjects, and the necessity of medical interventions. However, the latter
53 attract a significant portion of BCI research due to their safety, the lower equipment cost, and
54 the ability to collect large amount of data from patients and healthy participants. Specifically in
55 the case of electroencephalography (EEG), the added advantage of portability allows for the
56 inclusion of more subjects under more diverse and ecologically valid scenarios, therefore
57 making it currently one of the most attractive platforms.

58 Non-invasive BCI emerged in the early 90's [23–25], along with the first spatial filtering
59 algorithms. The Laplacian filter [26,27] allowed for improved signal-to-noise ratio, while the
60 common spatial pattern algorithm (CSP) [28–30] provided a way to weight the contribution of
61 each channel in order to optimize classification. Around the same time, a reliable, reproducible
62 signature of brain activity was demonstrated for the first time, at least on a trial-averaged level.
63 Studies in motor neuroscience involving healthy subjects revealed time-locked changes in
64 induced power within specific frequency bands [31–40]. Brain recordings were shown to exhibit
65 a gradual reduction in signal power, relative to baseline, in the mu (~ 8-12 Hz) and beta (~ 13-
66 30 Hz) frequency bands during an action or during motor imagery (MI): the so-called event-
67 related desynchronization (ERD). This phenomenon is considered to reflect processes related
68 to movement preparation and execution, and is particularly pronounced in the contralateral
69 sensorimotor cortex. Moreover, shortly following the completion of the task, a relative increase
70 in power, the event-related synchronization (ERS), could be observed in the beta band (also
71 referred to as the beta rebound). ERS is thought to reflect the re-establishment of inhibition in
72 the same area.

73 In the following years, the field witnessed the introduction of more advanced signal processing
74 methods [41], alternative non-invasive recording techniques [42,43] and hybrid BCI paradigms
75 [44–48]. During the past decade, attempts have been made to place more emphasis on the
76 user by studying individual traits that correlate with performance [49], or adapting BCI protocols
77 to the user [50–52] in an effort to better understand and mitigate the problem of BCI illiteracy [8]:
78 the inability of approximately 1/3 of the users to control a motor-imagery based BCI system.
79 Directly linked to this problem, there are significant efforts being made towards creating more
80 informative neurofeedback paradigms by studying the influence of feedback modality [53] and
81 factors not directly linked to the experimental task [54]. This multifaceted endeavor holds the
82 potential of considerably improving existing rehabilitation protocols [55].

83 Meanwhile, a great body of work has developed an arsenal of advanced pre-processing, feature
84 extraction, and classification algorithms dedicated specifically or adapted to the particular
85 characteristics and limitations of EEG signals [11,56]. As a first step, a standard BCI pipeline
86 includes dimensionality reduction techniques for channel selection and noise removal [57–59].
87 Subsequently, a common practice for signals recorded during MI or attempted movements is to
88 use a time-frequency (TF) transformation such as the short-time Fourier, Hilbert, or wavelet
89 transform [60–62] and extract the power of the signal in specific time windows and frequency
90 bands of interest. Finally, any of a large range of machine learning algorithms like linear
91 discriminant analysis (LDA) [63–65], support vector machines [66], random forests [67,68] or
92 neural networks [69] can be trained in order to establish a mapping between the features and
93 labels, and assess the performance of the whole pipeline.

94 This archetypical analysis is, to a significant extent, based on the idea that signal power is the
95 most informative signature of non-invasively recorded neural activity for motor-related tasks.
96 Ever since the characterization of the ERD and ERS phenomena, there has been little to no
97 discussion in the non-invasive BCI field as to whether these features accurately capture the
98 task-related modulations of brain activity. Recent studies in neurophysiology have challenged
99 this view and have demonstrated that the ERD and ERS patterns only emerge as a result of
100 averaging signal power over multiple trials [70,71]. On a single trial level, beta band activity
101 occurs in short, transient events, termed bursts, rather than as sustained oscillations [70–75].
102 This indicates that the ERD and ERS patterns reflect accumulated, time-varying changes in the
103 burst probability during each trial. Thus, beta bursts may carry more behaviorally relevant
104 information than averaged beta band power. Indeed, studies in humans involving arm
105 movements have established a link between the timing of sensorimotor beta bursts and
106 response times prior to movement, as well as behavioral errors post-movement [71]. Beta burst
107 activity in frontal areas has also been shown to correlate with movement cancellation [73,76,77]
108 and recent studies show that activity at the motor unit level also occurs in a transient manner,
109 which is time-locked to sensorimotor beta bursts [78,79].

110 Although beta burst rate has been shown to carry significant information, it still comprises a
111 rather simplistic representation of the underlying activity. Every burst can be characterized by a
112 set of TF-based features: the burst peak time and peak frequency, as well as its duration and its
113 span in the frequency axis [80]. In turn, all these descriptors are extracted using a particular
114 time-frequency transformation and constitute simpler representations of the more complex burst
115 waveform that is embedded in the raw signals, and which is characterized by a stereotypical
116 average shape with large variability around it [81]. The waveform features are neglected in
117 standard BCI approaches, because conventional signal processing methods generally
118 presuppose sustained, oscillatory and stationary signals, and are thus inherently unsuitable for
119 analyzing transient activity [82].

120 In line with the classically described ERD and ERS phenomena, the non-invasive BCI
121 community still heavily relies on signal power as the target feature for classification, although,
122 notably, state-of-the-art Riemannian classifiers [83–85] and some deep learning approaches
123 [86,87] have independently moved on from explicitly using frequency-specific power features. In
124 this article we propose a shift in perspective, by demonstrating how beta band activity during MI
125 tasks is modulated in terms of patterns of distinctly shaped bursts that are better descriptors of
126 transient activity changes.

127 We have previously argued that analyzing beta burst activity should enable us to gain access to
128 classification features that are at least as sensitive as beta band power [88]. If this hypothesis is
129 valid, then we should be able to test it and verify it using publicly available datasets. Here, we

130 show that this approach allows us to achieve better classification results than those obtained
131 when assessing signal power in binary MI classification tasks, when comparing burst features to
132 signal power from EEG channels C3 and C4. We validate our approach against six open EEG
133 BCI datasets, and provide links between the decoding performance and the modulation of
134 different features considered for classification across datasets and subjects. Although our
135 results obtained by using beta burst features are in most cases inferior to state-of-the-art,
136 namely because our analysis only included two channels and focused solely on the beta
137 frequency band, they are, conversely, superior to those obtained using only beta band power in
138 these channels. This analysis demonstrates the utility of beta burst analysis for BCI and paves
139 the way to improve classification performance in the near future.

140

141 **Materials and Methods**

142 **Datasets**

143 We used six open EEG MI datasets: BNCI 214-001 [89], BNCI 2014-004 [90], Cho 2017 [91],
144 MunichMI [92], Weibo 2014 [93] and Zhou 2016 [94], all available through the MOABB project
145 [95]. Briefly, all datasets contain recordings of subjects who were required to perform sustained
146 motor imagery following the appearance of a visual cue on a screen. For our analysis we only
147 considered trials corresponding to the “left hand” or “right hand” classes even if other classes
148 were available in some of the datasets.

149 **Data pre-processing**

150 For each dataset, recordings were loaded per subject using the MOABB python package
151 (v0.4.6) MotorImagery class, and were filtered with a low pass cutoff of 120 Hz. The low pass
152 cutoff was set to 95 Hz for the Weibo 2014 dataset, because the corresponding sampling
153 frequency of the recordings is 200 Hz. For most of these datasets numerous channels are
154 available, so we defined a subset of channels over the sensorimotor cortex that we deemed
155 relevant for the task and applied pre-processing (Table 1). Then, in this work, we only analyzed
156 data from channels C3 and C4. Each trial was aligned to the cue onset, and the task period was
157 defined as the time between cue onset and the end of the MI task. We used the time window
158 within one second prior to the cue onset as the baseline period (Table 1). In the case of the Cho
159 2017 and MunichMI datasets we noted the presence of noise at approximately 25 to 30 Hz that
160 interferes with the burst detection step. We therefore included an extra pre-processing step
161 involving a custom implementation of the meegkit python package (v0.1.3, dss_line function)
162 [96] to remove these artifacts. Considering only this subset of sensorimotor channels and all
163 recording periods, we rejected trials using the autoreject python package (0.4.0) [97] (Table 1).

164 **Identification of channel-specific beta band and burst detection**

165 Each subject's data were first transformed in the time-frequency domain from 1 to 43 Hz using
166 the superlets algorithm [98] with a frequency resolution of 0.5 Hz. We selected the superlets
167 algorithm over other more commonly used methods as it allows us to obtain a more optimal
168 tradeoff between temporal and spectral resolution, and because it has been shown to yield
169 better classification results compared to other approaches [99]. Before proceeding with any
170 further analysis we trimmed 200 to 250 ms from the beginning and end of the epoched data in
171 order to exclude any edge effects introduced by the time-frequency transform.

172 The power spectral density (PSD) of the baseline period was then computed by averaging the
173 resulting TF matrices over the temporal dimension for each trial and channel of a given subject.

174 Based on the distributions of the PSD peaks we attributed the peaks of the power spectra to
 175 either the mu (peaks below 15 Hz) or beta (peaks between 15 and 30 Hz) frequency band and
 176 proceeded by analyzing activity in the beta band.

Dataset	# Subjects	(# total channels) Channels used for pre- processing	# Total trials (# after trial rejection)	Baseline period (s)	Task period (s)	Post-task period (s)
BNCI 2014-001	9	(22) "FC3", "FCz", "FC4", "C3", "Cz", "C4", "CP3", "CPz", "CP4"	288 (207 - 287)	-1.0 - 0.0	0.0 - 4.0	4.0 - 5.5
BNCI 2014-004	9	(3) "C3", "Cz", "C4"	680 - 760 (269 - 621)	-1.0 - 0.0	0.0 - 4.5	4.5 - 6.5
Cho 2017	49	(64) "FC3", "FCz", "FC4", "C3", "Cz", "C4", "CP3", "CPz", "CP4"	200 - 240 (77 - 240)	-1.0 - 0.0	0.0 - 3.0	3.0 - 5.0
Munich MI	10	(13) "111", "112", "113", "114", "43", "21", "63", "22", "44", "119", "120", "121", "122"	300 (167 - 299)	-1.0 - 0.0	0.0 - 7.0	7.0 - 9.0
Weibo 2014	10	(60) "FC3", "FCz", "FC4", "C3", "Cz", "C4", "CP3", "CPz", "CP4"	140 - 160 (32 - 160)	-1.0 - 0.0	0.0 - 4.0	3.0 - 5.0
Zhou 2016	4	(64) "FC3", "FCz", "FC4", "C3", "Cz", "C4", "CP3", "CPz", "CP4"	290 - 319 (167 - 289)	-1.0 - 0.0	0.0 - 5.0	5.0 - 7.0

177 **Table 1.** Attributes of the datasets used in the study.

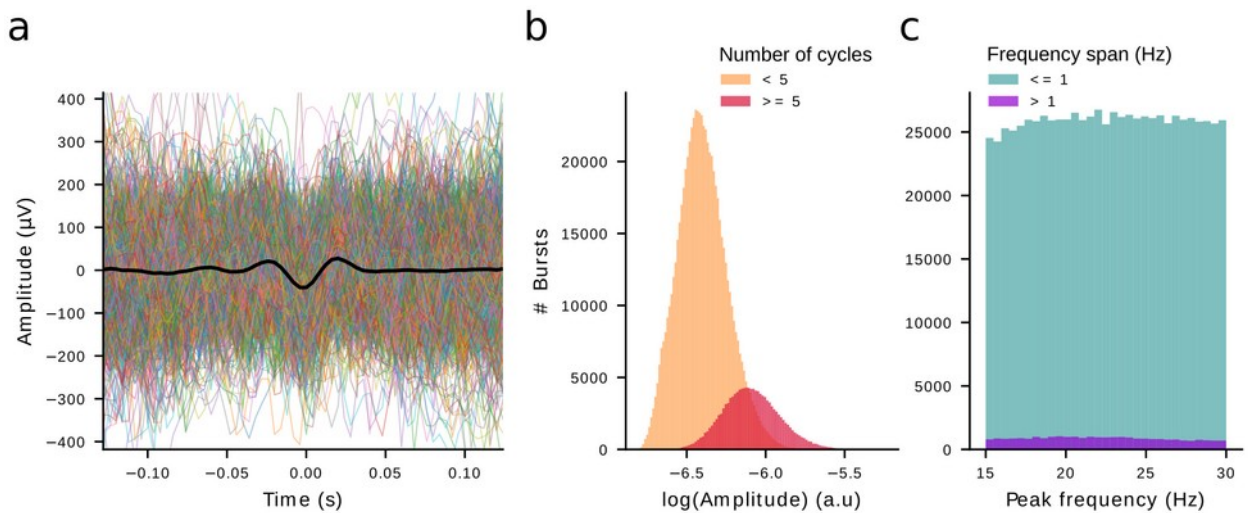
178 Using a previously published iterative, adaptive procedure, we identified bursts within the beta
 179 frequency range from the TF matrix, and then extracted their waveforms from the "raw" time
 180 series (after low pass filtering as pre-processing) within a fixed time window of 260 ms, centered
 181 on the burst peak [100]. Due to inability to parameterize spectra from all datasets we subtracted
 182 twice the standard deviation of the TF before fitting each peak as a 2D Gaussian, instead of
 183 subtracting the aperiodic activity from the TF matrices [81,101,102], before detecting beta
 184 bursts.

185 Feature extraction based on patterns of burst rate modulation

186 Beta burst waveform analysis was performed for each dataset by creating a dictionary of
 187 detected bursts across subjects and experimental conditions ("left hand" or "right hand") (figure
 188 1). This allowed us to create a matrix of burst waveforms by combining all detected bursts per
 189 subject, after robust scaling (scikit-learn package [103], v1.0.2). This representation of burst
 190 waveforms is suitable for applying a dimensionality reduction technique in order to better
 191 understand the variability in the recorded beta burst shapes. For the remaining of the analysis,
 192 we only considered channels C3 and C4, or channels 43 and 44 for the MunichMI dataset.

193 Previous work from our group has demonstrated that principal component analysis (PCA) [104]
 194 (scikit-learn package, v1.0.2) can be used to understand how the rates of bursts with different
 195 waveforms are modulated during reaching movements [100]. In order to construct features
 196 suitable for classification, we projected the burst dictionary along each principal component. As
 197 such, each burst was associated with a specific score along each dimension of the C-
 198 dimensional space, representing the distance of the burst's waveform from the average
 199 waveform of all bursts, along this dimension. Because of the scarcity of bursts with extreme
 200 scores, we winsorized scores outside of the 2nd and 98th percentile of their distribution. For each
 201 component, we then discretized the bursts into groups of bursts within equally spaced score

202 ranges, thus grouping bursts with similar waveforms along that dimension. Since each burst
203 occurs in a specific point in time, following this procedure all bursts were represented in a
204 subspace spanned by the dimensions of scores and time. In other words, for each principal
205 component we generated a representation of burst rate as a function of waveform shape.

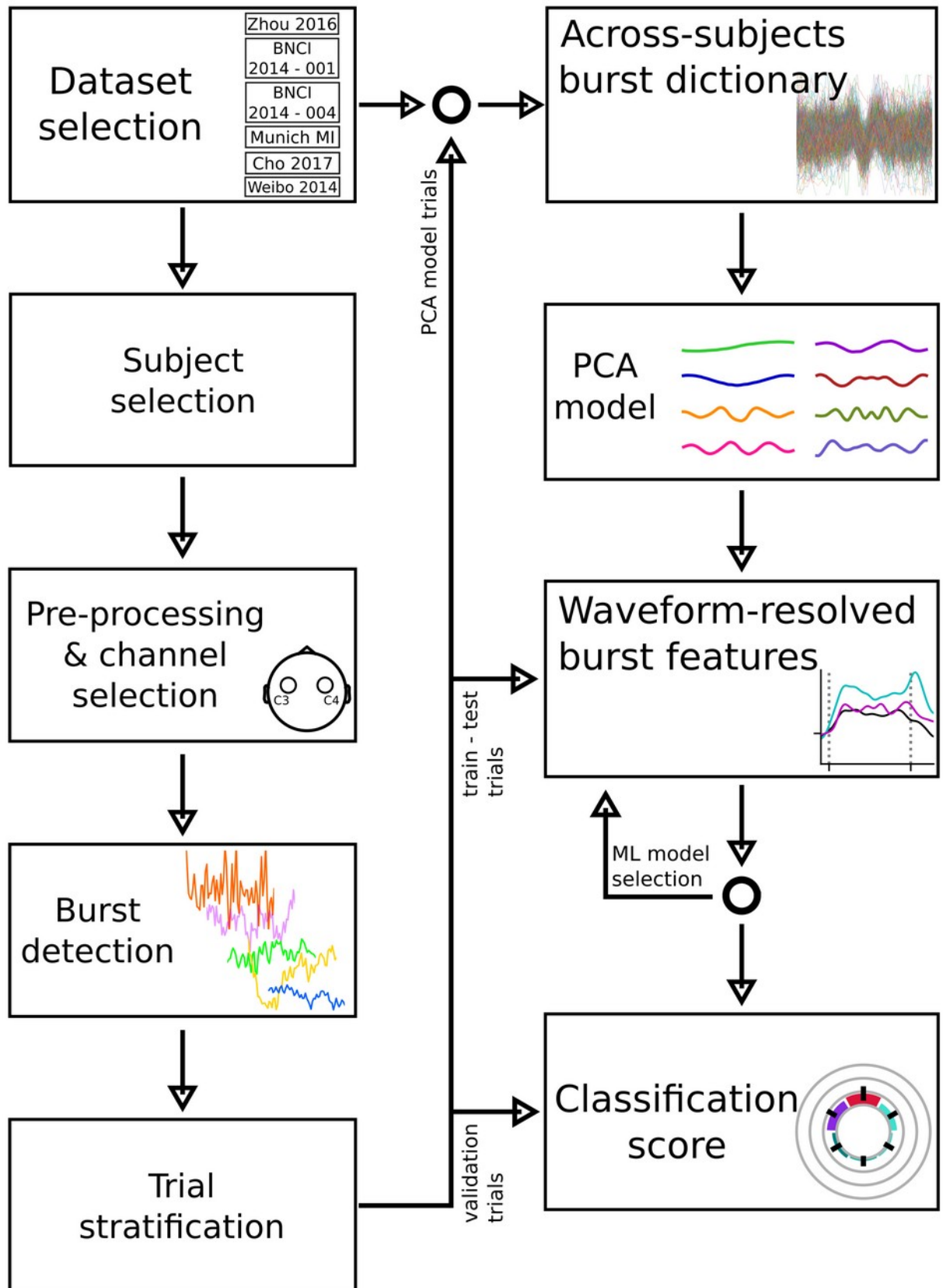


206 **Figure 1.** Burst dictionary corresponding to the Zhou 2016 dataset. **(a)** The dictionary contains raw, aligned signal
207 waveforms of 260 ms duration. The black trace represents the average waveform over the whole dictionary. Colored
208 traces correspond to a randomly drawn subset of waveforms (0.2% of all bursts). **(b)** Distribution of the TF amplitude
209 of bursts as computed by the superlets transform, grouped according to burst duration in terms of cycles. The burst
210 detection algorithm identifies a wide range of bursts with amplitudes spanning more than one order of magnitude.
211 The majority of detected beta bursts are low-power, short lasting events. **(c)** Distribution of the peak frequency
212 grouped by the frequency span of each burst. Most of the beta bursts have a narrow frequency span.

213

214 Classification

215 In order to obtain classification results with our beta burst waveform-based features, we used a
216 stratified, repeated cross-validation approach. For each dataset, we first randomized the trials'
217 order and stratified the total number of trials of each subject in $M=5$ strata. Then, we used half
218 of the trials of one stratum for creating an across-subjects burst dictionary, ran PCA on the
219 resulting waveform matrix and kept track of the rest of the stratum's trials for cross validating the
220 decoding results. For each subject separately, we then projected the bursts of the remaining
221 four strata (the trials not used during the burst dictionary creation step or for cross validation)
222 along each component and, after averaging the burst rate of each group during the task period,
223 we employed a repeated cross validation with $K=5$ folds. For each fold we repeated this
224 procedure for 100 repetitions by shuffling the order of the features. In order to obtain the results
225 for this analysis, we iterated over a number of possible groups (*from 2 to 9*) and principal
226 components (*from 1 to 8*). We report the maximum classification score in this hyper-parameter
227 space after cross validating each stratum and averaging across all M strata. All steps of the
228 analysis are summarized in a flowchart (figure 2).



229 **Figure 2.** Flowchart illustrating the steps of the proposed analysis. For each dataset, we iteratively pre-processed the
230 data of each subject, rejecting trials and keeping only channels C3 and C4. The burst detection algorithm was run on
231 the raw signals of these two channels. We, then split the remaining trials of each subject in 3 sets. The first set was
232 used only to create the burst dictionary and the corresponding PCA model combining data from all subjects of any
233 given dataset. The second set was used as the training and testing set of trials, in order to select the best model of

234 waveform-resolved features, in terms of decoding score, through a nested, repeated cross validation procedure.
235 Finally, the third set of trials served the role of the validation trials, for the previously selected model.

236 We compared these results against decoding results obtained by using other related
237 approaches. First, classification results based on beta burst rate were computed for each
238 subject by sampling all detected bursts of channels C3 and C4, and then identifying the rate of
239 bursts within the time course of a trial in non-overlapping time windows of 100 ms. For these
240 results, we only considered bursts with an amplitude equal to or higher than the 75th percentile
241 of the dictionary's TF amplitude distribution, a threshold commonly used when detecting beta
242 bursts with alternative methods [75,105–108].

243 We also estimated the decoding accuracy based on TF-based features of the bursts as
244 determined by the burst detection algorithm. We used an approach similar to that described for
245 constructing features and estimating classification results based on burst waveforms.
246 Specifically, for each subject we identified all bursts of channels C3 and C4 and computed the
247 binned burst rate based on the burst volume, burst amplitude, or the combination of TF
248 features, namely burst amplitude, peak frequency, FWHM duration, and FWHM frequency span.
249 We again explored from 2 to 9 possible number of burst groups for each of these features in a
250 repeated, 5-fold cross validation (sup. figure 1).

251 Band power results for the beta band were based on the power of the Hilbert transform of
252 channels C3 and C4 only. Recordings were first band-pass filtered using the same beta
253 frequency range per channel (15 to 30 Hz). These results are based on a repeated cross-
254 validation approach, and only take into account activity during the task period. The classification
255 features were repeatedly shuffled 100 times, then, for each repetition the trials were split in $K=5$
256 folds.

257 All classification results were obtained by using LDA as a classifier (scikit-learn, v1.0.2). We
258 estimated the classification score based on the area under the curve (AUC) of the receiver
259 operating characteristic (scikit-learn, v1.0.2). All numeric computations were based on the
260 numpy python package (v1.21.6; [109]), an environment running python (v3.10). We compared
261 trial-level classification results of the waveform-resolved burst features to the beta band power
262 features using a generalized linear mixed model with a binomial distribution and logit link
263 function with correct classification of each trial as the dependent variable, the type of
264 classification feature as a fixed effect, and the subject nested within the dataset as random
265 intercepts. We also compared classification results of the waveform-resolved burst features to
266 the rest of the burst features using a similar model. Statistical analyses were conducted using R
267 (v4.1.2) and lme4 (v1.1-31; [110]). Fixed effects were assessed using type II Wald X^2 tests
268 using car (v3.1-1; [111]). Pairwise Tukey-corrected follow-up tests were carried out using
269 estimated marginal means from the emmeans package (v.1,8,7 [112]).

270

271 **Results**

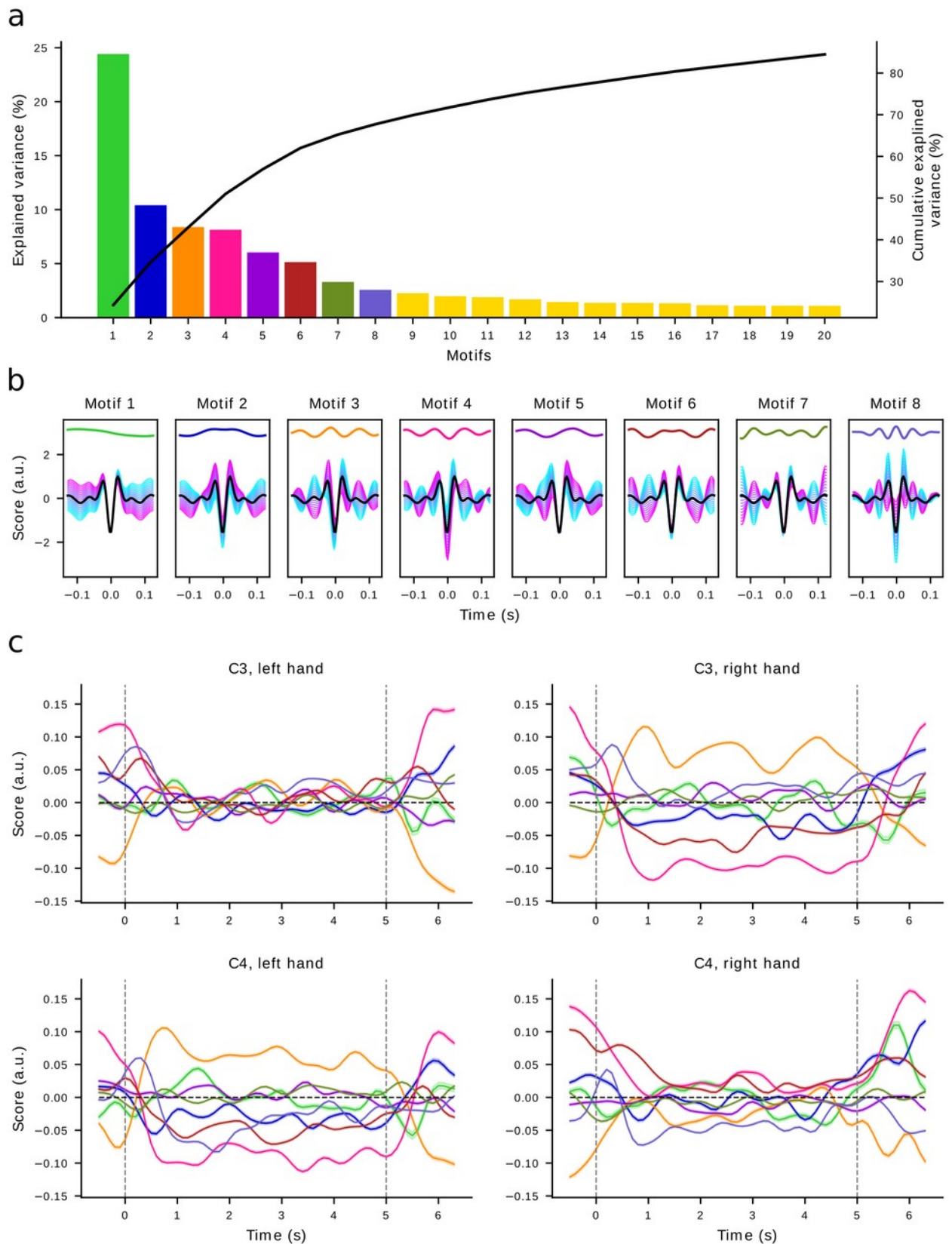
272 We used six open MI EEG datasets for the purpose of examining the explanatory value of beta
273 burst activity as a feature for BCI classification. For each dataset, we detected beta bursts in a
274 subset of channels over the sensorimotor cortex under two conditions, “left hand” and “right
275 hand” MI. Based on the bursts detected in channels C3 and C4 of each subject, we built
276 dataset-specific burst dictionaries which capture the variability of the burst waveforms (figure 1)
277 (see Materials and Methods).

278 **Beta bursts with distinct waveforms are characterized by different modulation patterns**

279 We used principal component analysis (PCA) to explain the variability of the burst waveforms
280 within each dictionary (number of components explaining 99% of variance). This method
281 allowed us to reduce the dimensionality of the burst waveform space, with each resulting
282 dimension being a linear combination of the burst waveforms, that emphasizes specific time
283 points that best describe the waveform variability (figure 3 a). Every component defines a motif,
284 along which the waveforms vary. The projection of a burst waveform along each component,
285 associates this waveform with a score, a value that indicates its similarity to the average
286 waveform of bursts within the dictionary along that dimension.

287 We simulated how each motif alters the waveform with respect to the average by varying the
288 score along each dimension, adding the weighted eigenvector to the mean waveform (figure 3
289 b) in order to understand how the burst waveform is modulated by the first 8 motifs. For
290 example, the first motif represents a trend that describes how the waveforms are temporally
291 skewed. Motifs 5, 6 and 7 mainly capture the variability along the flanks of the waveform,
292 whereas motifs 2, 3 and 4 seem to describe changes of the central negative deflection.

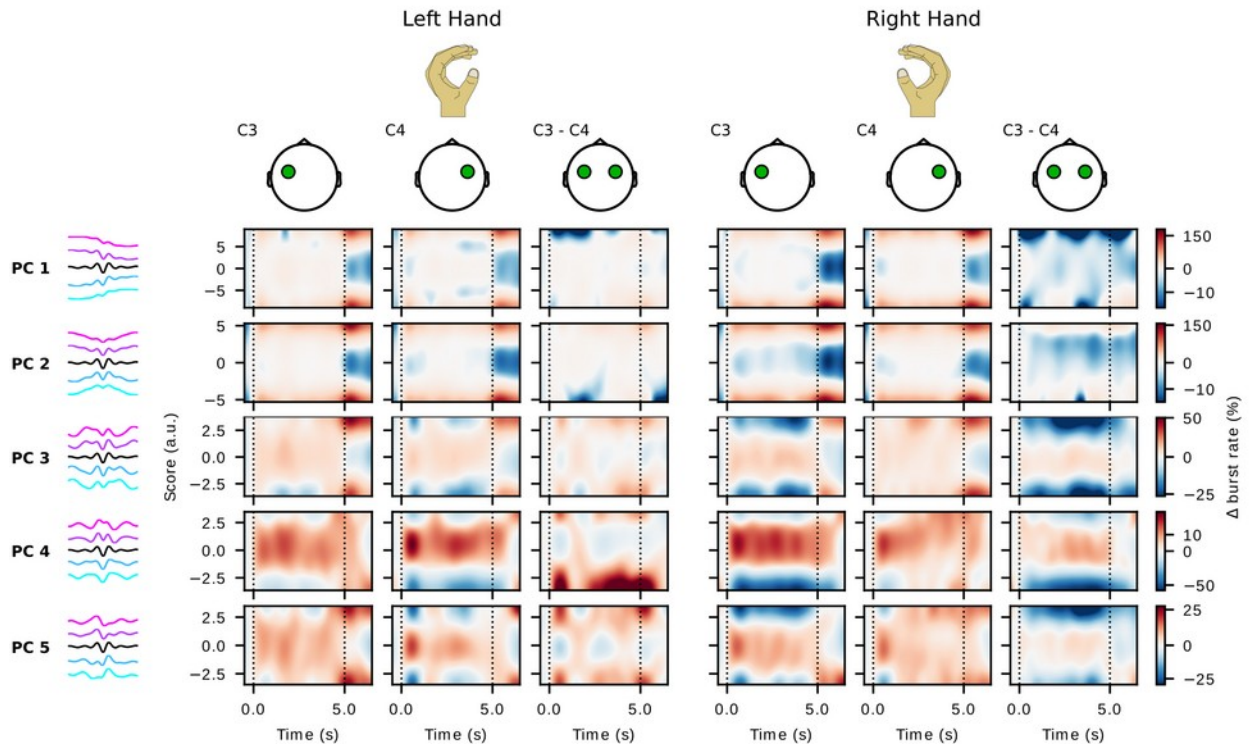
293 For each condition, channel and component we computed the average score of all bursts within
294 the burst dictionary from the baseline to the post-task period, and applied a smoothing kernel of
295 size 2. Burst scores in specific motifs were modulated to different extents within the three trial
296 periods: baseline, task and post-task period (figure 3 c). This means that, on average, bursts
297 with different waveforms occurred more or less frequently within specific trial periods (e.g. motif
298 4). However, a change in mean waveform shape is ambiguous with respect to the underlying
299 mechanism: e.g. over contralateral motor cortex there was a pronounced decrease in score
300 along component 4 during the task, but this could be due to a reduction in the rate of bursts with
301 high scores, an increase in the rate of bursts with negative scores, or a combination of the two.



302 **Figure 3.** PCA applied on the burst dictionary of the Zhou 2016 dataset. Principal components describe the variability
303 of burst waveforms. **(a)** Ratio of explained variance and cumulative explained variance for the first 20 components.
304 **(b)** The first 8 components define orthogonal axes of waveform shape alteration with respect to the average
305 waveform (black trace). Each subplot depicts one motif (color code as in **a**), the mean waveform (black trace), and
306 simulated waveform alterations along each component, spanning a continuous space from negative (cyan traces) to
307 positive (magenta traces) scores. **(c)** Average score and standard error of all waveforms along each component
308 during the three trial periods for the first 8 components (color code as in **a**) for each condition and channel. During the
309 baseline and post-task periods (signified by the vertical dashed lines), waveforms deviate from the average waveform

310 (score equal to 0) mainly along the third and fourth dimension ipsilaterally, while contralaterally the deviation is more
311 pronounced during the task period.

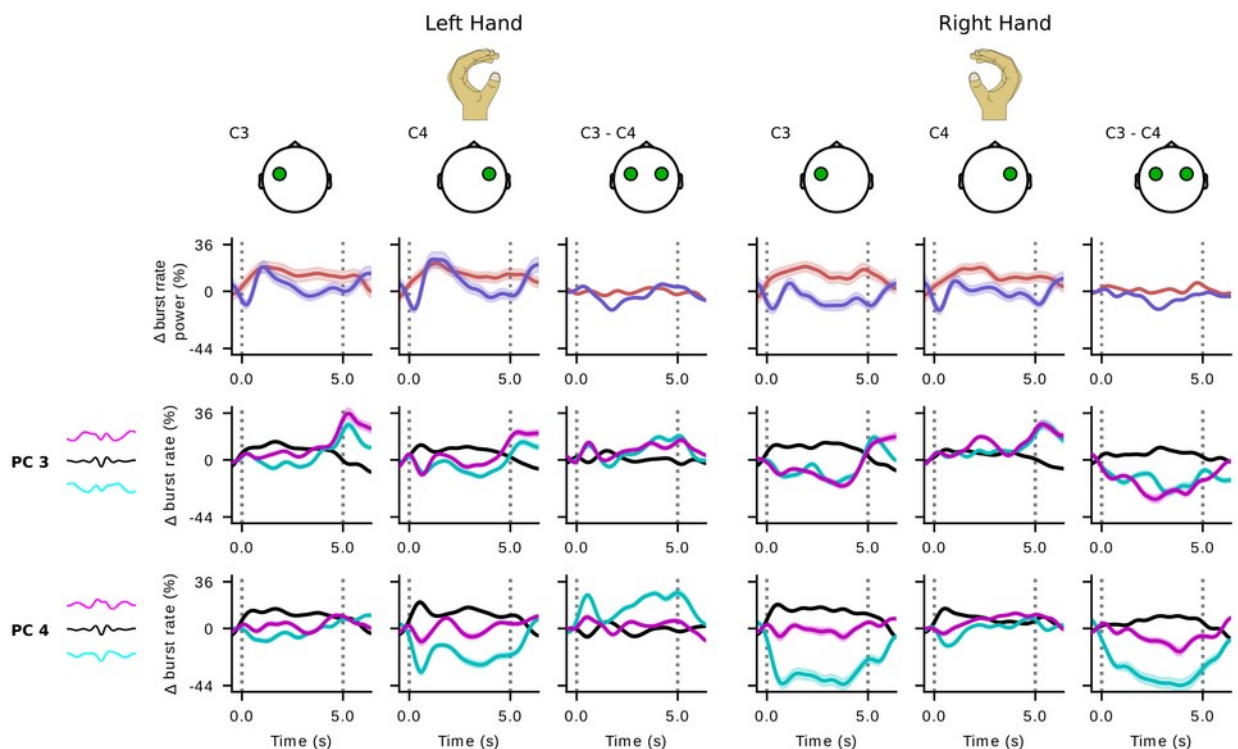
312 To better understand the rate modulation of bursts with distinct waveforms along each
313 component over all experimental periods, we visualized the trial-averaged, baseline-corrected
314 burst rate as a function of time and component score, for the first five components of a
315 representative subject (figure 4; Zhou 2016 dataset, S1). In this particular case there were
316 differences in burst rate modulation between channels C3 and C4, as well as between the two
317 experimental conditions. During the task period there was a decrease in the rate of bursts with
318 large positive or negative scores along component 4 on the contralateral channel for either
319 condition. These patterns correspond to bursts whose waveforms resemble the corresponding
320 magenta and cyan traces. The lateralization of beta burst rate modulation is further exemplified
321 when visualizing the difference between the two channels. The comparison of these differences
322 across the two conditions, reveals that all components and especially components 3, 4 and 5
323 encode disparities between the “left hand” and “right hand” conditions, and could therefore
324 constitute informative features for a classifier. Interestingly, some components seem to describe
325 a modulation of waveforms during the post-task period, which is particularly evident for either
326 condition in components 1 and 2.



327 **Figure 4.** Trial-averaged, baseline-corrected burst rate along different components for a representative subject (Zhou
328 2016, S1). The first column depicts how burst waveforms vary independently along each component (components as
329 depicted in figure 3). Negative scores correspond to the cyan traces, and positive to the magenta traces. The
330 average waveform is represented by the black trace. During “left hand” trials, burst rate varies per component for
331 channels C3 and C4 and the difference of the two channels. During the task period, both channels exhibit various
332 degrees of burst rate increase for bursts whose waveforms resemble the average along any principal component.
333 Waveforms lying further from the average along component 3 and more prominently 4 are characterized by a
334 reduction of burst rate contralaterally, in channel C4. Similar patterns arise for the “right hand” trials. Component 5 is
335 characterized by an ipsilateral increase and a contralateral decrease of “positive outlier” waveforms. During the post-
336 task period a burst rate increase for specific waveforms is observed, mainly seen along components 1 and 2.

337 **Beta band burst features outperform beta band power in binary classification tasks**

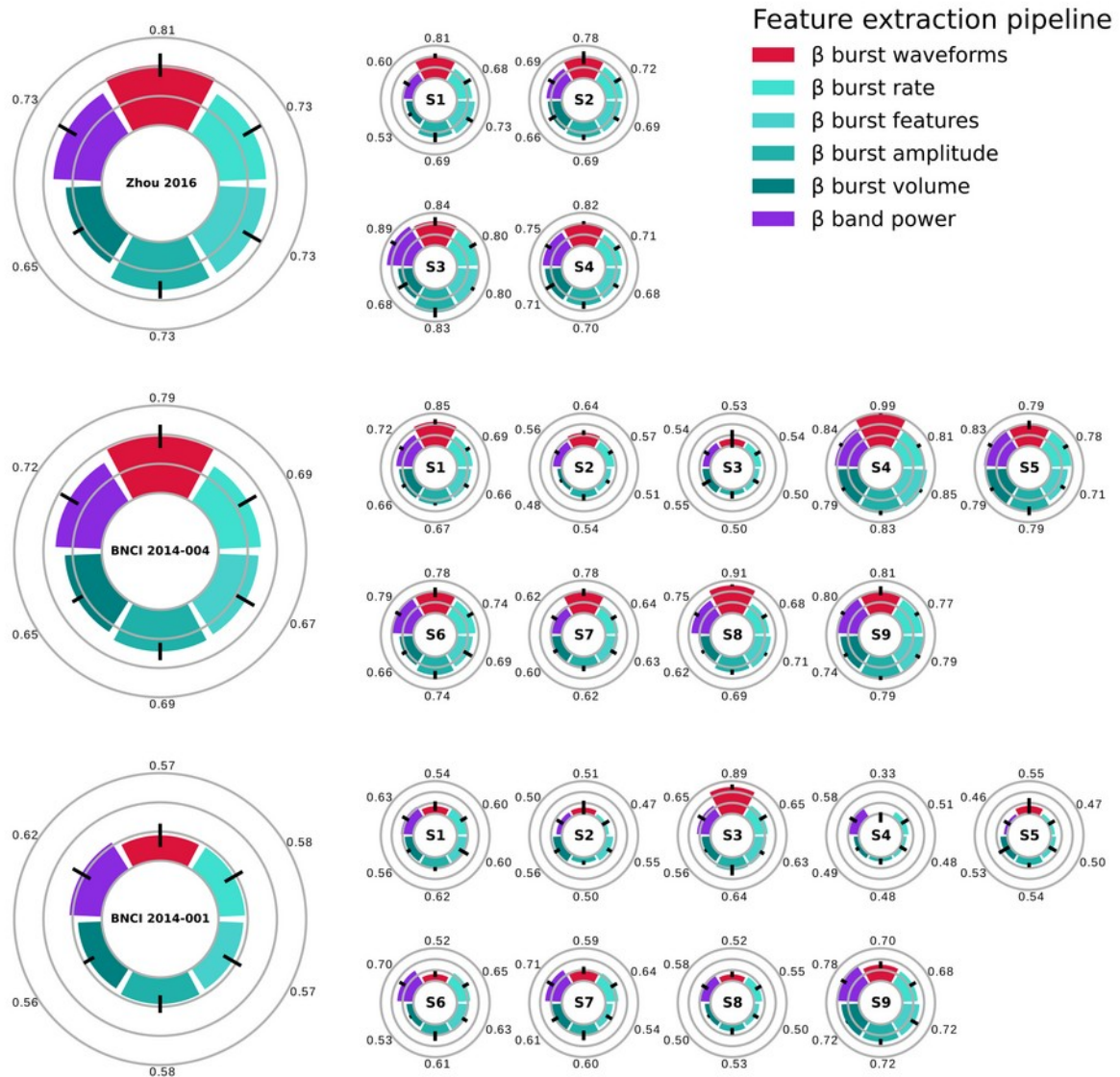
338 After establishing the lower dimensional space for projecting the burst waveforms, we binned
339 the scores axis into several groups per component (figure 5) using a cross-validation procedure,
340 and analyzed the average burst rate per group (see Materials and Methods). The average burst
341 rate for each group during the task period within each of the two channels was then used as a
342 feature for an LDA classifier, resulting in $G \times C \times 2$ features per experimental condition, where G
343 is the number of groups, and C is the number of components, e.g. in the two bottom lines of figure
344 5 we visualize what would correspond to $G=3$ and $C=2$. In order to validate our hypothesis, we
345 compared classification results based on this method against results based on alternative
346 features: the overall beta burst rate for bursts detected in channels C3 and C4 and whose
347 amplitude is greater than a threshold (the 75th percentile of the dictionary's TF amplitude
348 distribution); time-frequency descriptions of bursts, and band power in the beta frequency (see
349 Materials and Methods).



350 **Figure 5.** Trial-averaged, baseline-corrected overall burst rate, beta band power and burst rate modulation of three
351 burst groups along components 3 and 4 for a representative subject (Zhou 2016 dataset, S1). For both conditions and channels, beta band power changes (purple trace) roughly track the overall burst rate modulation (red trace).
352 and channels, beta band power changes (purple trace) roughly track the overall burst rate modulation (red trace).
353 Burst rate modulation for different burst groups varies per condition, channel and component. The differential
354 modulation of burst rate is particularly pronounced contralaterally, in channel C4 during "left hand" trials and channel
355 C3 during "right hand" trials along the fourth component. A clear distinction between conditions is evident when
356 comparing the difference of rate modulation of the two channels for each waveform group.

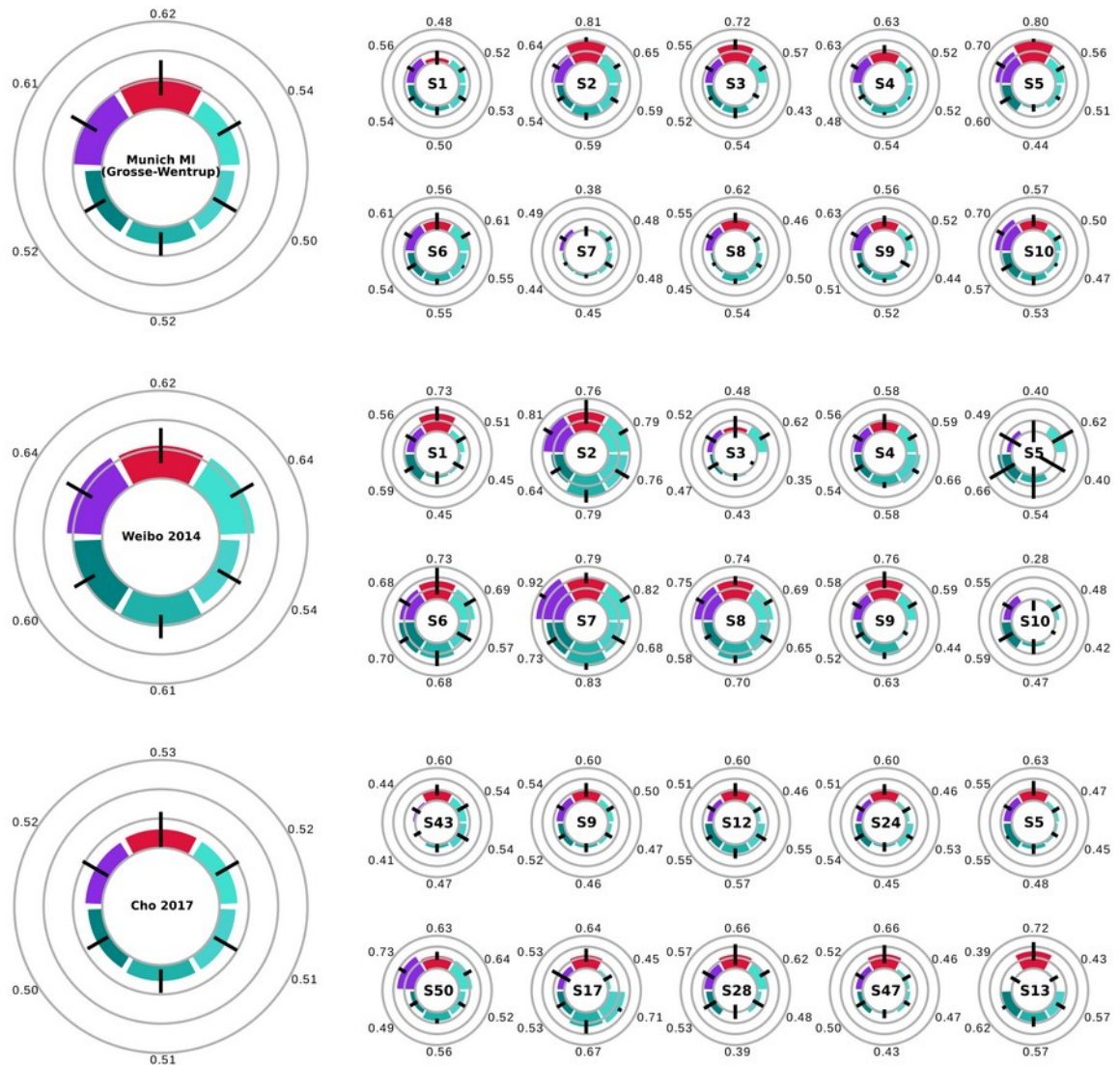
357 For each dataset we present the across-subject average results estimated with each method,
358 as well as the results for each participant (figures 6, 7). For the Cho 2017 dataset, which
359 contains a large number of participants, we only show the best ten subjects according to the
360 results based on burst waveform features. The results of all subjects are provided separately
361 (sup. figure 2). At the dataset level, the waveform-resolved burst rate features yield decoding
362 results that are equivalent or better than the results obtained by analyzing beta band power, or
363 alternative beta band representations. These representations appear to bear analogous results
364 in each dataset. We emphasize, though, that the results are highly variable across subjects. For
365 example, for subject S1 of the Zhou 2016 dataset beta power does not hold much explanatory
366 value, unlike beta burst rate, beta burst amplitude or the waveform-resolved burst rate. This is

367 not true for S4 of the BNCI 2014-004 dataset. All representations yield similarly good results,
 368 except for the waveform-resolved burst rate that outperforms the rest.



369 **Figure 6.** Population average and individual results for binary “left hand” vs “right hand” classification for the BNCI
 370 2014-001, BNCI 2014-004 and Zhou 2016 and datasets. Classification features based on burst waveform-specific
 371 rate yield, on average, better results than those obtained using TF-derived burst features, or beta power from
 372 channels C3 and C4 across all datasets

373 After obtaining these results we proceeded to quantify the statistical significance of the
 374 observed differences for each classification feature set. In order to test the explanatory value of
 375 the waveform-resolved burst rate against beta band power we analyzed the decoding results
 376 using a generalized linear mixed model (see Materials and Methods). The waveform-resolved
 377 burst rate features are significantly better than beta band power features ($X^2(1) = 21.384, p <$
 378 0.001). We also compared the waveform-resolved burst rate against the rest of the examined
 379 beta band representations and verified that it yields the highest classification accuracy ($X^2(4) =$
 380 242.95 , all pairwise $p < 0.001$). In conclusion, we confirmed our hypothesis that waveform-
 381 resolved beta burst activity holds promise to improve BCI performance, especially if further
 382 optimized so that it can be analyzed online and take into account multiple recording channels.



383 **Figure 7.** Population average and individual results for binary “left hand” vs “right hand” classification for the Cho
384 2017, Munich MI (Grosse-Wentrup) and Weibo 2014 datasets. Only the 10 best subjects according to burst waveform
385 features are shown for the Cho 2017 dataset. All features yield equivalent results for the Cho 2017 dataset. Burst
386 waveforms and band power features are equivalent and superior to other beta band activity representations for the
387 Munich Mi dataset. All beta band features except for the combination of multiple features, yield similar results for the
388 Weibo 2014 dataset. Color code as in figure 6.

389

390 Discussion

391 In this study, we showed for the first time that waveform-specific beta burst rate is a
392 representation comparable to beta power within a framework of binary classification MI tasks. In
393 an attempt to understand why, we compared multiple representations of beta activity modulation
394 during the MI task. We showed that bursts of different shapes are selectively modulated
395 following task onset, with distinct waveforms occurring with different probability during different
396 points in time [100] (figures 4 and 5). This modulation can be encoded either by TF-derived
397 features, or alternatively, burst waveforms. All of the TF-derived features were as informative as
398 the overall burst rate when used as classification features, but less reliable than waveform-
399 based features, across all datasets.

400 The results presented in this article are based on features of beta bursts detected from only two
401 channels, and are therefore not directly comparable to results of previous studies that have
402 implemented standard designs within the BCI literature [95,113] and incorporate all available
403 recording channels, do not perform trial rejection, and utilize spatial filtering. However,
404 waveform-based burst rate features are more informative about imagined movements than beta
405 power in channels C3 and C4. In this regard, our analysis is a first step in the direction of
406 establishing a neurophysiologically informed alternative to currently existing methodologies of
407 feature extraction.

408 Our results rely on burst dictionaries that combine data from all subjects across a dataset. We
409 have introduced this “transfer learning-like” approach because we have observed that it makes
410 the dimensionality reduction step less susceptible to noise and it results in the same
411 components for all subjects within a dataset, thus rendering the classification features and
412 decoding results easier to interpret. Additionally, it is worth mentioning that due to the enforced
413 orthogonality between the PCA dimensions, the resulting principal components are similar to a
414 Fourier decomposition of the time series, which may be suboptimal by failing to capture
415 components that optimally separate bursts that are differently modulated by the task.
416 Conversely, this property of PCA imposes restrictions on the resulting components that make
417 them similar across datasets (sup. figure 4). This property could be taken advantage of and
418 used in future work for cross-dataset transfer learning.

419 An important question is whether this procedure would be suitable for online, real-time
420 decoding. The superlets algorithm, and to a lesser extent the burst detection algorithm, are
421 computationally expensive and increasing the number of recording channels, task duration, and
422 frequency resolution would make it difficult to employ this analysis online. However, our results
423 show that beta bursts with particular waveforms are more informative of MI than others. These
424 waveforms could be used as kernels and convolved with online recordings to efficiently detect
425 bursts directly in the time domain. If burst waveforms are maintained across recording sessions,
426 the superlets-based burst analysis could be performed during an offline session and its results
427 used for online burst detection during follow-up, online sessions.

428 Although we observe distinct patterns of beta burst rate modulations during trials, we do not
429 know how these patterns evolve over sessions and whether or not they are affected by learning.
430 Likewise, how these patterns are influenced by various brain disorders and diseases remains to
431 be studied. There is evidence that beta burst activity is profoundly altered in Parkinson’s
432 disease [75,105,106,114,115], and it could be hypothesized that the alterations in beta band
433 activity following stroke [116–118] may be linked to changes in beta burst waveforms as well.
434 To answer these questions, a longitudinal comparison between a healthy population and clinical
435 patients is needed to establish a link between behavioral or clinical changes and the recorded
436 waveform-specific burst rate patterns or other beta activity representations. Beta burst
437 waveforms could thus serve as an alternative bio-marker for neurofeedback paradigms, and
438 particularly neurorehabilitation protocols.

439 Tremendous efforts to improve the reliability of non-invasive BCI have been so far unable to
440 provide solutions that would be acceptable for widely-adopted applications. Ever since the
441 characterization of the event-related synchronization and desynchronization phenomena of mu
442 and beta activity, little effort has been put into revisiting the features that are considered to best
443 capture the underlying brain activity in these BCI paradigms. Growing evidence suggests that
444 beta activity modulations are best described in terms of bursts. The analysis presented in this
445 study serves as a proof of concept for the proposed methodology, but there is significant
446 potential for improvement in the burst detection and feature creation procedures. Future

447 directions of interest lie in incorporating more advanced spatial filtering with the burst detection
448 technique, and possibly the use of state-of-the-art Riemannian methods, so that we can
449 leverage the activity of more channels within this framework. Finally, another future direction lies
450 in the incorporation of novel neurophysiological markers for the mu frequency band in our
451 framework. A growing number of studies have shown that the activity in this band can occur as
452 longer-lasting bursts [119], or non-sinusoidal oscillations [120]. We believe that by adapting our
453 approach to the characteristics of this frequency band, or by adopting alternative frameworks
454 such as cycle-by-cycle analysis [121] we can uncover features that will further help us attain the
455 goal of improving BCI robustness. We believe all these goals to be particularly interesting
456 because they hold the promise of further improving current results and rendering them
457 comparable to state-of-the-art approaches.

458

459 **Conclusion**

460 Waveform-resolved patterns of burst rate constitute a new way of analyzing beta band activity
461 during motor imagery tasks. The assessment of this method against multiple open EEG
462 datasets shows that this representation is better than conventional power features in terms of
463 classification. This work serves as a first step and opens up numerous directions for further
464 improvements that can potentially ameliorate the reliability of existing, non-invasive brain-
465 computer interface technology.

466

467 **Acknowledgments**

468 This work was performed within the framework of the LABEX CORTEX (ANR-11LABX-0042) of
469 Université de Lyon, within the program “Investissements d’Avenir” (decision n° 2019-ANR-
470 LABX-02) operated by the French National Research Agency (ANR). SP, MC, JB, and JM are
471 supported by the French National Research Agency (ANR) project HiFi (2020–2024). MS and
472 JB are supported by the European Research Council (ERC) under the European Union’s
473 Horizon 2020 Research and Innovation Programme (ERC consolidator grant 864550 to JB).

474

475 **Data availability Statement**

476 All data are available via the [MOABB project](#). All scripts necessary for reproducing the results of
477 this article are available at the following public repository: <https://gitlab.com/sotpapad/bebopbci>.

478

479 **Author Contributions**

480 SP, JB and JM conceptualized the manuscript. SP drafted the manuscript and performed the
481 analysis. All authors contributed to manuscript revision, read, and approved the submitted
482 version.

483

484 **Competing Interest Statement**

485 All authors declare no competing interests.

486

487 **References**

488

- 489 [1] Kurzweil R 2014 The Singularity is Near *Ethics and Emerging Technologies* ed R L
490 Sandler (London: Palgrave Macmillan UK) pp 393–406
- 491 [2] Wolpaw J R 2002 Brain Computer Interfaces for communication and control *Front.*
492 *Neurosci.* **4** 767–91
- 493 [3] Wolpaw J R, Millán J del R and Ramsey N F 2020 Brain-computer interfaces: Definitions
494 and principles *Handb. Clin. Neurol.* **168** 15–23
- 495 [4] Ramadan R A and Vasilakos A V. 2017 Brain computer interface: control signals review
496 *Neurocomputing* **223** 26–44
- 497 [5] Lotte F, Nam C S and Nijholt A 2018 Introduction : Evolution of Brain-Computer
498 Interfaces *Technol. Theor. Adv. Taylor Fr. (CRC Press.* **9781498773** 1–11
- 499 [6] Hatsopoulos N G and Donoghue J P 2009 The Science of Neural Interface Systems
500 *Annu. Rev. Neurosci.* **32** 249–66
- 501 [7] Mueller-Putz G, Scherer R, Brunner C, Leeb R and Pfurtscheller G 2008 Better than
502 random: A closer look on BCI results *Int. J. Bioelectromagn.* **10** 52–5
- 503 [8] Vidaurre C and Blankertz B 2010 Towards a cure for BCI illiteracy *Brain Topogr.* **23** 194–
504 8
- 505 [9] Chavarriaga R, Fried-Oken M, Kleih S, Lotte F and Scherer R 2016 Heading for new
506 shores! Overcoming pitfalls in BCI design *Brain-Computer Interfaces* **4** 60–73
- 507 [10] Hughes C, Herrera A, Gaunt R and Collinger J 2020 *Bidirectional brain-computer*
508 *interfaces* vol 168 (Elsevier B.V.)
- 509 [11] Iturrate I, Chavarriaga R and Millán J del R 2020 General principles of machine learning
510 for brain-computer interfacing *Handb. Clin. Neurol.* **168** 311–28
- 511 [12] Blokland Y, Spyrou L, Thijssen D, Eijsvogels T, Colier W, Floor-Westerdijk M, Vlek R,
512 Bruhn J and Farquhar J 2014 Combined EEG-fNIRS decoding of motor attempt and
513 imagery for brain switch control: An offline study in patients with tetraplegia *IEEE Trans.*
514 *Neural Syst. Rehabil. Eng.* **22** 222–9
- 515 [13] Saeedi S, Chavarriaga R and Millan J D R 2017 Long-Term Stable Control of Motor-
516 Imagery BCI by a Locked-In User Through Adaptive Assistance *IEEE Trans. Neural Syst.*
517 *Rehabil. Eng.* **25** 380–91
- 518 [14] Benaroch C, Sadatnejad K, Roc A, Appriou A, Monseigne T, Pramij S, Mladenovic J,
519 Pillette L, Jeunet C and Lotte F 2021 Long-Term BCI Training of a Tetraplegic User:
520 Adaptive Riemannian Classifiers and User Training *Front. Hum. Neurosci.* **15** 1–22
- 521 [15] Baniqued P D E, Stanyer E C, Awais M, Alazmani A, Jackson A E, Mon-Williams M A,
522 Mushtaq F and Holt R J 2021 Brain–computer interface robotics for hand rehabilitation
523 after stroke: a systematic review *J. Neuroeng. Rehabil.* **18** 1–25

- 524 [16] Luauté J, Morlet D and Mattout J 2015 BCI in patients with disorders of consciousness:
525 Clinical perspectives *Ann. Phys. Rehabil. Med.* **58** 29–34
- 526 [17] Mane R, Wu Z and Wang D 2022 Poststroke motor, cognitive and speech rehabilitation
527 with brain-computer interface: A perspective review *Stroke Vasc. Neurol.* **7** 541–9
- 528 [18] Chaudhary U, Birbaumer N and Ramos-Murguialday A 2016 *Brain-computer interfaces*
529 *in the completely locked-in state and chronic stroke* vol 228 (Elsevier B.V.)
- 530 [19] McFarland D J 2021 Brain-computer interfaces for amyotrophic lateral sclerosis Dennis
531 *Muscle Nerve* **61** 702–7
- 532 [20] Bai Z, Fong K N K, Zhang J J, Chan J and Ting K H 2020 Immediate and long-term
533 effects of BCI-based rehabilitation of the upper extremity after stroke: A systematic
534 review and meta-analysis *J. Neuroeng. Rehabil.* **17** 1–20
- 535 [21] Tam W, Wu T, Zhao Q, Keefer E and Yang Z 2019 Human motor decoding from neural
536 signals: a review *BMC Biomed. Eng.* **1** 1–22
- 537 [22] Willett F R, Avansino D T, Hochberg L R, Henderson J M and Shenoy K V. 2021 High-
538 performance brain-to-text communication via handwriting *Nature* **593** 249–54
- 539 [23] Farwell L A and Donchin E 1988 Talking off the top of your head: toward a mental
540 prosthesis utilizing event-related brain potentials *Electroencephalogr. Clin. Neurophysiol.*
541 510–23
- 542 [24] Wolpaw J R, McFarland D J, Neat G W and Forneris C A 1991 An EEG-based brain-
543 computer interface for cursor control *Electroencephalogr. Clin. Neurophysiol.* **78** 252–9
- 544 [25] Pfurtscheller G, Flotzinger D and Kalcher J 1993 Brain-Computer Interface-a new
545 communication device for handicapped persons *J. Microcomput. Appl.* **16** 293–9
- 546 [26] Lu J, McFarland D J and Wolpaw J R 2013 Adaptive laplacian filtering for sensorimotor
547 rhythm-based brain-computer interfaces *J. Neural Eng.* **10**
- 548 [27] McFarland D J, McCane L M, David S V. and Wolpaw J R 1997 Spatial filter selection for
549 EEG-based communication *Electroencephalogr. Clin. Neurophysiol.* **103** 386–94
- 550 [28] Koles Z J 1991 The quantitative extraction and topographic mapping of the abnormal
551 components in the clinical EEG *Electroencephalogr. Clin. Neurophysiol.* **79** 440–7
- 552 [29] Blankertz B, Kawanabe M, Tomioka R, Hohlefeld F U, Nikulin V and Müller K R 2008
553 Invariant common spatial patterns: Alleviating nonstationarities in Brain-Computer
554 Interfacing *Adv. Neural Inf. Process. Syst. 20 - Proc. 2007 Conf.* 1–8
- 555 [30] Müller-Gerking J, Pfurtscheller G and Flyvbjerg H 1999 Designing optimal spatial filters
556 for single-trial EEG classification in a movement task *Clin. Neurophysiol.* **110** 787–98
- 557 [31] Pfurtscheller G and Lopes da Silva F H 1999 Event-related EEG/MEG synchronization
558 and desynchronization: basic principles *Clin. Neurophysiol.* **110** 1842–57
- 559 [32] Pfurtscheller G and Neuper C 1997 Motor imagery activates primary sensorimotor area
560 in humans *Neurosci. Lett.* **239** 65–8
- 561 [33] Pfurtscheller G and Berghold A 1989 Patterns of cortical activation during planning of
562 voluntary movement *Electroencephalogr. Clin. Neurophysiol.* **72** 250–8

- 563 [34] Pfurtscheller G, Stancák A and Neuper C 1996 Post-movement beta synchronization. A
564 correlate of an idling motor area? *Electroencephalogr. Clin. Neurophysiol.* **98** 281–93
- 565 [35] Pfurtscheller G, Brunner C, Schlögl A and Lopes da Silva F H 2006 Mu rhythm
566 (de)synchronization and EEG single-trial classification of different motor imagery tasks
567 *Neuroimage* **31** 153–9
- 568 [36] Neuper C, Wörtz M and Pfurtscheller G 2006 Chapter 14 ERD/ERS patterns reflecting
569 sensorimotor activation and deactivation *Prog. Brain Res.* **159** 211–22
- 570 [37] Pfurtscheller G, Neuper C, Flotzinger D and Pregenzer M 1997 EEG-based
571 discrimination between imagination of right and left hand movement *Electroencephalogr.*
572 *Clin. Neurophysiol.* **103** 642–51
- 573 [38] Alayrangues J, Torrecillos F, Jahani A and Malfait N 2019 Error-related modulations of
574 the sensorimotor post-movement and foreperiod beta-band activities arise from distinct
575 neural substrates and do not reflect efferent signal processing *Neuroimage* **184** 10–24
- 576 [39] Cheyne D and Ferrari P 2013 MEG studies of motor cortex gamma oscillations:
577 Evidence for a gamma “fingerprint” in the brain? *Front. Hum. Neurosci.* **7** 1–7
- 578 [40] Kilavik B E, Zaepffel M, Brovelli A, MacKay W A and Riehle A 2013 The ups and downs
579 of beta oscillations in sensorimotor cortex *Exp. Neurol.* **245** 15–26
- 580 [41] Makeig S, Enghoff S, Jung T P and Sejnowski T J 2000 A natural basis for efficient
581 brain-actuated control *IEEE Trans. Rehabil. Eng.* **8** 208–11
- 582 [42] Waldert S, Preissl H, Demandt E, Braun C, Birbaumer N, Aertsen A and Mehring C 2008
583 Hand movement direction decoded from MEG and EEG *J. Neurosci.* **28** 1000–8
- 584 [43] Naseer N and Hong K S 2015 fNIRS-based brain-computer interfaces: A review *Front.*
585 *Hum. Neurosci.* **9** 1–15
- 586 [44] Allison B Z, Brunner C, Kaiser V, Müller-Putz G R, Neuper C and Pfurtscheller G 2010
587 Toward a hybrid brain-computer interface based on imagined movement and visual
588 attention *J. Neural Eng.* **7**
- 589 [45] Sadeghi S and Maleki A 2018 Recent advances in hybrid brain-computer interface
590 systems: A technological and quantitative review *Basic Clin. Neurosci.* **9** 373–88
- 591 [46] Buccino A P, Keles H O and Omurtag A 2016 Hybrid EEG-fNIRS asynchronous brain-
592 computer interface for multiple motor tasks *PLoS One* **11** 1–16
- 593 [47] Choi I, Rhiu I, Lee Y, Yun M H and Nam C S 2017 A systematic review of hybrid brain-
594 computer interfaces: Taxonomy and usability perspectives *PLoS One* **12**
- 595 [48] Corsi M C, Chavez M, Schwartz D, Hugueville L, Khambhati A N, Bassett D S and De
596 Vico Fallani F 2019 Integrating EEG and MEG Signals to Improve Motor Imagery
597 Classification in Brain-Computer Interface *Int. J. Neural Syst.* **29** 1–12
- 598 [49] Lotte F and Rimbart S 2022 How ERD modulations during motor imageries relate to
599 users’ traits and BCI performances *44th International Engineering in Medicine and*
600 *Biology Conference* (Glasgow, United Kingdom)

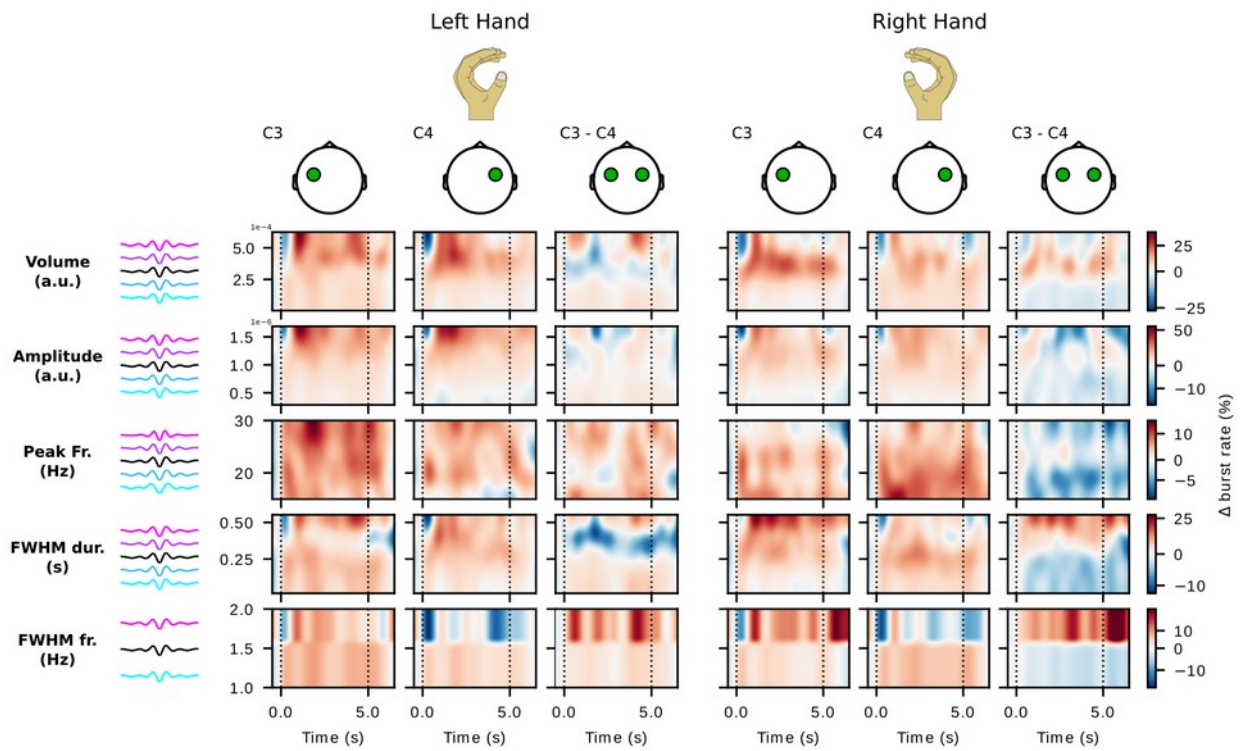
- 601 [50] Lotte F, Jeunet C, Mladenovic J, Kaoua B N and A L P 2018 A BCI challenge for the
602 signal processing community : considering the user in the loop *Signal Processing and*
603 *Machine Learning for Brain-Machine Interfaces* pp 1–33
- 604 [51] Mladenović J, Frey J, Pramij S, Mattout J and Lotte F 2022 Towards Identifying Optimal
605 Biased Feedback for Various User States and Traits in Motor Imagery BCI *IEEE Trans.*
606 *Biomed. Eng.* **69** 1101–10
- 607 [52] Mladenović J 2021 Standardization of protocol design for user training in EEG-based
608 brain-computer interface *J. Neural Eng.* **18**
- 609 [53] Pillette L, N'kaoua B, Sabau R, Glize B and Lotte F 2021 Multi-Session Influence of Two
610 Modalities of Feedback and Their Order of Presentation on MI-BCI User Training
611 *Multimodal Technol. Interact. MDPI* **5** 12
- 612 [54] Jeunet C, Lotte F, Batail J M, Philip P and Micoulaud Franchi J A 2018 Using Recent
613 BCI Literature to Deepen our Understanding of Clinical Neurofeedback: A Short Review
614 *Neuroscience* **378** 225–33
- 615 [55] Jeunet C, Glize B, McGonigal A, Batail J M and Micoulaud-Franchi J A 2019 Using EEG-
616 based brain computer interface and neurofeedback targeting sensorimotor rhythms to
617 improve motor skills: Theoretical background, applications and prospects *Neurophysiol.*
618 *Clin.* **49** 125–36
- 619 [56] Lotte F, Bougrain L, Cichocki A, Clerc M, Congedo M, Rakotomamonjy A and Yger F
620 2018 A review of classification algorithms for EEG-based brain-computer interfaces: A 10
621 year update *J. Neural Eng.* **15**
- 622 [57] Zarei R, He J, Siuly S and Zhang Y 2017 A PCA aided cross-covariance scheme for
623 discriminative feature extraction from EEG signals *Comput. Methods Programs Biomed.*
624 **146** 47–57
- 625 [58] Kachenoura A, Albera L, Senhadji L and Comon P 2008 ICA: A potential tool for BCI
626 systems *IEEE Signal Process. Mag.* **25** 57–68
- 627 [59] Medeiros de Freitas A, Sanchez G, Lecaigard F, Maby E, Barbosa Soares A and
628 Mattout J 2020 EEG artifact correction strategies for online trial-by-trial analysis *J. Neural*
629 *Eng.* **17**
- 630 [60] Bruns A 2004 Fourier-, Hilbert- and wavelet-based signal analysis: Are they really
631 different approaches? *J. Neurosci. Methods* **137** 321–32
- 632 [61] Herman P, Prasad G, McGinnity T M and Coyle D 2008 Comparative analysis of spectral
633 approaches to feature extraction for EEG-based motor imagery classification *IEEE Trans.*
634 *Neural Syst. Rehabil. Eng.* **16** 317–26
- 635 [62] Brodu N, Lotte F and Lécuyer A 2011 Comparative study of band-power extraction
636 techniques for Motor Imagery classification *IEEE SSCI 2011 - Symp. Ser. Comput. Intell.*
637 *- CCMB 2011 2011 IEEE Symp. Comput. Intell. Cogn. Algorithms, Mind, Brain* 95–100
- 638 [63] Pfurtscheller G and Neuper C 2001 Motor imagery direct communication *Proc. IEEE* **89**
639 1123–34

- 640 [64] Vidaurre C, Kawanabe M, Von Bünau P, Blankertz B and Müller K R 2011 Toward
641 unsupervised adaptation of LDA for brain-computer interfaces *IEEE Trans. Biomed. Eng.*
642 **58** 587–97
- 643 [65] Llera A, Gomez V and Kappen H J 2014 Adaptive Multiclass Classification for Brain
644 Computer Interfaces *Neural Comput.* **26** 1108–27
- 645 [66] Song X, Yoon S C and Perera V 2013 Adaptive Common Spatial Pattern for single-trial
646 EEG classification in multisubject BCI *Int. IEEE/EMBS Conf. Neural Eng. NER* **19013**
647 411–4
- 648 [67] Steyrl D, Scherer R, Oswin F and Gernot R M 2014 Motor Imagery Brain-Computer
649 Interfaces : Random Forests vs Regularized LDA - Non-linear Beats Linear *Proc. 6th Int.*
650 *Brain-Computer Interface Conf.* 8–11
- 651 [68] Steyrl D, Scherer R, Faller J and Müller-Putz G R 2016 Random forests in non-invasive
652 sensorimotor rhythm brain-computer interfaces: A practical and convenient non-linear
653 classifier *Biomed. Tech.* **61** 77–86
- 654 [69] Hazrati M K and Erfanian A 2010 An online EEG-based brain-computer interface for
655 controlling hand grasp using an adaptive probabilistic neural network *Med. Eng. Phys.* **32**
656 730–9
- 657 [70] Jones S R 2016 When brain rhythms aren't 'rhythmic': implication for their mechanisms
658 and meaning *Curr. Opin. Neurobiol.* **40** 72–80
- 659 [71] Little S, Bonaiuto J, Barnes G and Bestmann S 2019 Human motor cortical beta bursts
660 relate to movement planning and response errors *PLoS Biol.* **17** 1–30
- 661 [72] Lundqvist M, Rose J, Herman P, Brincat S, Buschman T and Miller E 2016 Gamma and
662 beta bursts underlie working memory *Neuron* **90** 152–64
- 663 [73] Wessel J R 2020 B-Bursts Reveal the Trial-To-Trial Dynamics of Movement Initiation
664 and Cancellation *J. Neurosci.* **40** 411–23
- 665 [74] Shin H, Law R, Tsutsui S, Moore C I and Jones S R 2017 The rate of transient beta
666 frequency events predicts impaired function across tasks and species *Elife*
- 667 [75] Torrecillos F, Tinkhauser G, Fischer P, Green A L, Aziz T Z, Foltynie T, Limousin P,
668 Zrinzo L, Ashkan K, Brown P and Tan H 2018 Modulation of beta bursts in the
669 subthalamic nucleus predicts motor performance *J. Neurosci.* **38** 8905–17
- 670 [76] Hannah R, Muralidharan V, Sundby K K and Aron A R 2020 Temporally-precise
671 disruption of prefrontal cortex informed by the timing of beta bursts impairs human action-
672 stopping *Neuroimage* **222**
- 673 [77] Enz N, Ruddy K L, Rueda-Delgado L M and Whelan R 2021 Volume of β -bursts, but not
674 their rate, predicts successful response inhibition *J. Neurosci.* **41** 5069–79
- 675 [78] Bräcklein M, Barsakcioglu D Y, Vecchio A Del and Ibáñez J 2022 Reading and
676 Modulating Cortical β Bursts from Motor Unit Spiking Activity **42** 3611–21
- 677 [79] Echeverria-altuna I, Quinn A J, Woolrich M W, Nobre A C and Ede V 2022 Transient
678 beta activity and cortico-muscular connectivity during sustained motor behaviour *Prog.*
679 *Neurobiol.* 102281

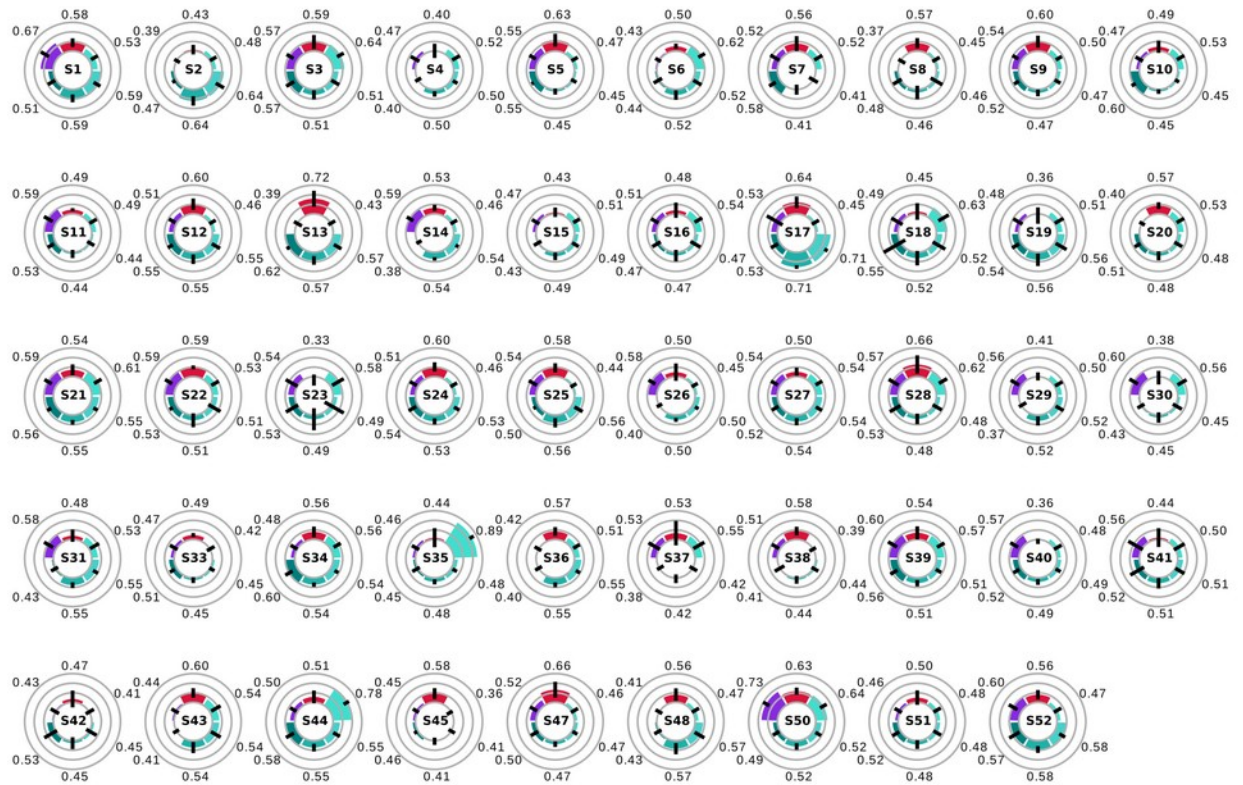
- 680 [80] Zich C, Quinn A J, Bonaiuto J J, O'Neill G, Mardell L C, Ward N S and Bestmann S 2023
681 Spatiotemporal organization of human sensorimotor beta burst activity *Elife* **12:e80160**
- 682 [81] Szul M J, Papadopoulos S, Alavizadeh S, Daligaut S, Schwartz D, Mattout J and
683 Bonaiuto J J 2023 Diverse beta burst waveform motifs characterize movement-related
684 cortical dynamics *Prog. Neurobiol.* 165187
- 685 [82] Donoghue T, Schaworonkow N and Voytek B 2021 Methodological considerations for
686 studying neural oscillations *Eur. J. Neurosci.* 1–26
- 687 [83] Barachant A, Bonnet S, Congedo M and Jutten C 2012 Multiclass Brain-Computer
688 Interface Classification by Riemannian Geometry *IEEE Trans. Biomed. Eng.* **59** 920–8
- 689 [84] Barachant A, Bonnet S, Congedo M and Jutten C 2013 Classification of covariance
690 matrices using a Riemannian-based kernel for BCI applications *Neurocomputing* **112**
691 172–8
- 692 [85] Congedo M, Barachant A and Bhatia R 2017 Riemannian geometry for EEG-based
693 brain-computer interfaces; a primer and a review *Brain-Computer Interfaces* **4** 155–74
- 694 [86] Roy Y, Banville H, Albuquerque I, Gramfort A, Falk T H and Faubert J 2019 Deep
695 learning-based electroencephalography analysis: A systematic review *J. Neural Eng.* **16**
- 696 [87] Kwon O Y, Lee M H, Guan C and Lee S W 2020 Subject-Independent Brain-Computer
697 Interfaces Based on Deep Convolutional Neural Networks *IEEE Trans. Neural Networks*
698 *Learn. Syst.* **31** 3839–52
- 699 [88] Papadopoulos S, Bonaiuto J and Mattout J 2022 An Impending Paradigm Shift in Motor
700 Imagery Based Brain-Computer Interfaces *Front. Neurosci.* **15**
- 701 [89] Tangermann M, Müller K R, Aertsen A, Birbaumer N, Braun C, Brunner C, Leeb R,
702 Mehring C, Miller K J, Müller-Putz G R, Nolte G, Pfurtscheller G, Preissl H, Schalk G,
703 Schlögl A, Vidaurre C, Waldert S and Blankertz B 2012 Review of the BCI competition IV
704 *Front. Neurosci.* **6** 1–31
- 705 [90] Leeb R, Lee F, Keinrath C, Scherer R, Bischof H and Pfurtscheller G 2007 Brain-
706 computer communication: motivation, aim, and impact of exploring a virtual apartment.
707 *IEEE Trans. neural Syst. Rehabil. Eng. a Publ. IEEE Eng. Med. Biol. Soc.* **15** 473–82
- 708 [91] Cho H, Ahn M, Ahn S, Kwon M and Jun S C 2017 EEG datasets for motor imagery
709 brain-computer interface *Gigascience* **6** 1–8
- 710 [92] Grosse-Wentrup M, Liefhold C, Gramann K and Buss M 2009 Beamforming in
711 Noninvasive Brain-Computer Interfaces *IEEE Trans. Biomed. Eng.* **56** 1209–19
- 712 [93] Yi W, Qiu S, Wang K, Qi H, Zhang L, Zhou P, He F and Ming D 2014 Evaluation of EEG
713 oscillatory patterns and cognitive process during simple and compound limb motor
714 imagery *PLoS One* **9** 1–19
- 715 [94] Zhou B, Wu X, Lv Z, Zhang L and Guo X 2016 A fully automated trial selection method
716 for optimization of motor imagery based Brain-Computer interface *PLoS One* **11** 1–20
- 717 [95] Jayaram V and Barachant A 2018 MOABB: Trustworthy algorithm benchmarking for
718 BCIs *J. Neural Eng.* **15**

- 719 [96] de Cheveigné A 2020 ZapLine: A simple and effective method to remove power line
720 artifacts *Neuroimage* **207**
- 721 [97] Jas M, Engemann D A, Bekhti Y, Raimondo F, Gramfort A, Gramfort A, Automated A
722 and Engemann D A 2017 Autoreject : Automated artifact rejection for MEG and EEG data
723 *Neuroimage* **159** 417–129
- 724 [98] Moca V V., Bârzan H, Nagy-Dăbâcan A and Mureşan R C 2021 Time-frequency super-
725 resolution with superlets *Nat. Commun.* **12** 1–18
- 726 [99] Bârzan H, Ichim A M, Moca V V and Mureşan R C 2022 Time-Frequency
727 Representations of Brain Oscillations: Which One Is Better? *Front. Neuroinform.* **16** 1–14
- 728 [100] Szul M J, Papadopoulos S, Alavizadeh S, Daligaut S, Schwartz D, Mattout J and
729 Bonaiuto J J 2022 Diverse beta burst waveform motifs characterize movement-related
730 cortical dynamics *bioRxiv*
- 731 [101] Brady B and Bardouille T 2022 Periodic/Aperiodic parameterization of transient
732 oscillations (PAPTO)—Implications for healthy ageing *Neuroimage* **251** 118974
- 733 [102] Rodriguez-Larios J and Haegens S 2023 Genuine beta bursts in human working
734 memory: controlling for the influence of lower-frequency rhythms *bioRxiv*
735 2023.05.26.542448
- 736 [103] Pedregosa F, Varoquaux G, Gramfort A, Michel V, Thirion B, Grisel O, Blondel M,
737 Prettenhofer P, Weiss R, Bubourg V, Vanderplas J, Passos A, Cournapeau D, Brucher
738 M, Perrot M and Duchesnay E 2011 Scikit-learn: Machine Learning in Python Fabian J.
739 *Mach. Learn. Res.* **12** 2825–30
- 740 [104] Shlens J 2014 A Tutorial on Principal Component Analysis *arXiv*
- 741 [105] Tinkhauser G, Pogosyan A, Little S, Beudel M, Herz D M, Tan H and Brown P 2017 The
742 modulatory effect of adaptive deep brain stimulation on beta bursts in Parkinson's
743 disease *Brain* **140** 1053–67
- 744 [106] Tinkhauser G, Pogosyan A, Tan H, Herz D M, Kühn A A and Brown P 2017 Beta burst
745 dynamics in Parkinson's disease off and on dopaminergic medication *Brain* **140** 2968–81
- 746 [107] Khawaldeh S, Tinkhauser G, Shah S A, Peterman K, Debove I, Khoa Nguyen T A,
747 Nowacki A, Lenard Lachenmayer M, Schuepbach M, Pollo C, Krack P, Woolrich M and
748 Brown P 2020 Subthalamic nucleus activity dynamics and limb movement prediction in
749 Parkinson's disease *Brain* **143** 582–6
- 750 [108] Lofredi R, Neumann W J, Bock A, Horn A, Huebl J, Siegert S, Schneider G H, Krauss J
751 K and Kühn A A 2018 Dopamine-dependent scaling of subthalamic gamma bursts with
752 movement velocity in patients with Parkinson's disease *Elife* **7** 1–22
- 753 [109] Harris C R, Millman K J, van der Walt S J, Gommers R, Virtanen P, Cournapeau D,
754 Wieser E, Taylor J, Berg S, Smith N J, Kern R, Picus M, Hoyer S, van Kerkwijk M H, Brett
755 M, Haldane A, del Río J F, Wiebe M, Peterson P, Gérard-Marchant P, Sheppard K,
756 Reddy T, Weckesser W, Abbasi H, Gohlke C and Oliphant T E 2020 Array programming
757 with NumPy *Nature* **585** 357–62
- 758 [110] Bates D, Mächler M, Bolker B M and Walker S C 2015 Fitting linear mixed-effects
759 models using lme4 *J. Stat. Softw.* **67**

- 760 [111] Fox J and Weisberg S 2019 *An R Companion to Applied Regression* (Sage)
- 761 [112] Lenth R V 2023 emmeans: Estimated Marginal Means, aka Least-Squares Means
- 762 [113] Luiz P, Rodrigues C, Jutten C and Congedo M 2019 Riemannian Procrustes Analysis :
763 Transfer Learning for Brain-Computer Interfaces *IEEE Trans. Biomed. Eng.* **66** 2390–401
- 764 [114] Yeh C H, Al-Fatly B, Kühn A A, Meidahl A C, Tinkhauser G, Tan H and Brown P 2020
765 Waveform changes with the evolution of beta bursts in the human subthalamic nucleus
766 *Clin. Neurophysiol.* **131** 2086–99
- 767 [115] Jackson N, Cole S R, Voytek B and Swann N C 2019 Characteristics of waveform shape
768 in Parkinson's disease detected with scalp electroencephalography *eNeuro* **6** 1–11
- 769 [116] Rossiter H E, Boudrias M H and Ward N S 2014 Do movement-related beta oscillations
770 change after stroke? *J. Neurophysiol.* **112** 2053–8
- 771 [117] Shiner C T, Tang H, Johnson B W and McNulty P A 2015 Cortical beta oscillations and
772 motor thresholds differ across the spectrum of post-stroke motor impairment, a
773 preliminary MEG and TMS study *Brain Res.* **1629** 26–37
- 774 [118] Kulasingham J P, Brodbeck C, Khan S, Marsh E B and Simon J Z 2022 Bilaterally
775 Reduced Rolandic Beta Band Activity in Minor Stroke Patients *Front. Neurol.* **13** 1–10
- 776 [119] Vigué-Guix I and Soto-Faraco S 2022 Using occipital α -bursts to modulate behaviour in
777 real-time *bioRxiv*
- 778 [120] Chen Y Y, Lambert K J M, Madan C R and Singhal A 2021 Mu oscillations and motor
779 imagery performance: A reflection of intra-individual success, not inter-individual ability
780 *Hum. Mov. Sci.* **78** 1–12
- 781 [121] Cole S and Voytek B 2019 Cycle-by-cycle analysis of neural oscillations *J.*
782 *Neurophysiol.* **122** 849–61



783 **Sup. Figure 1.** Trial-averaged, baseline-corrected burst rate along different TF-derived features for a representative
784 subject (Zhou 2016 dataset, S1).



785 **Sup. Figure 2.** Results for binary “left hand” vs “right hand” classification for all subjects of the Cho 2017 dataset.
786 Color code as in figure 6.